

Understanding microbiome dynamics via interpretable graph representation learning

Kateryna Melnyk^{a,*}, Kuba Weimann^b and Tim O.F. Conrad^b

^aDepartment of Mathematics and Computer Science, Freie Universität Berlin, Arnimallee 6, Berlin, 14195, Germany

^bZuse Institute Berlin, Takustraße 7, Berlin, 14195, Germany

ARTICLE INFO

Keywords:

Graph representation learning
Dynamical systems
Biological network
Microbiome

ABSTRACT

Large-scale perturbations in the microbiome constitution are strongly correlated, whether as a driver or a consequence, with the health and functioning of human physiology. However, understanding the difference in the microbiome profiles of healthy and ill individuals can be complicated due to the large number of complex interactions among microbes. We propose to model these interactions as a time-evolving graph whose nodes are microbes and edges are interactions among them. Motivated by the need to analyse such complex interactions, we develop a method that learns a low-dimensional representation of the time-evolving graph and maintains the dynamics occurring in the high-dimensional space. Through our experiments, we show that we can extract graph features such as clusters of nodes or edges that have the highest impact on the model to learn the low-dimensional representation. This information can be crucial to identify microbes and interactions among them that are strongly correlated with clinical diseases. We conduct our experiments on both synthetic and real-world microbiome datasets.

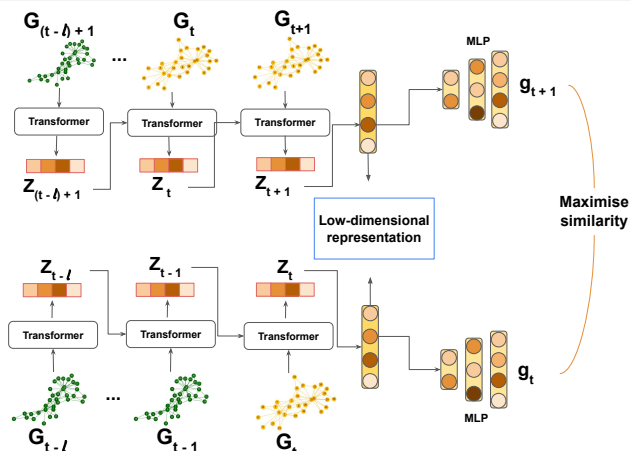


Figure 1: Overview of the method proposed in this paper to learn the embedding of the time-evolving graph.

1. Introduction

Complex microbiome ecosystems have a strong impact on the health and functioning of human physiology. Large-scale perturbations in the microbiome constitution are strongly correlated, whether as a driver or a consequence, with clinical diseases, such as inflammatory bowel disease [19, 24], obesity [23], and some types of cancer [33, 27, 6, 4].

Many studies have been aimed at accurately differentiating the disease state and at understanding the difference in the microbiome profiles of healthy and ill individuals [25, 3]. However, most of them mainly focus on various statistical approaches, omitting microbe-microbe interactions between a large number of microbiome taxa that, in principle, drive microbiome dynamics. In addition, some

studies make use of the concept of a potential landscape in physics [5, 30, 12], giving a completely new insight into the analysis of microbiome dynamics. Namely, a healthy human microbiome can be considered as a metastable state lying in a minimum of some potential landscape. The system of time-evolving interactions of species appears to be equilibrated for a short timescale but at larger timescales a disease or other strongly impacting factors, such as antibiotic exposure, makes the system undergo transitions from one metastable state (healthy) to other metastable states (diseased).

Detecting metastable states and associated interactions of species, which undergo changes from one metastable state to others, is complicated by the high dimensionality and the compositional nature of microbiome data. Therefore, we propose a method that simplifies analysis and prediction of the large-scale dynamics of microbiome composition by projecting this system onto a low-dimensional space. First, to allow interactions between species to change over time, we represent the system as a time-evolving graph with nodes being microbes and edges being interactions between microbes. Second, we define two key components of our method: 1) the Transformer [35] that learns both structural patterns of the time-evolving graph and temporal changes of the microbiome system, and 2) contrastive learning that makes the model maintain metastability in a low-dimensional space. To assess the performance of our method, we apply it to the synthetic data from [22], which has known underlying dynamics, and to two real-world microbiome datasets, i.e. MovingPic [3] and Cholera Infection [17]. Furthermore, we will show that it is feasible to extract topological features of the time-evolving graph which are associated with metastable states and have the highest impact on how the model learns the low-dimensional representation of the time-evolving graph with metastability.

*Corresponding author

 melnykk96@zedat.fu-berlin.de (K. Melnyk)

This information can help in differentiating the microbiome profile of healthy and diseased individuals.

Contribution. Overall, this paper makes the following contributions:

- We present a model that learns a low-dimensional representation of the time-evolving graph in an unsupervised manner. Through our experiments, we demonstrate that the metastability governing the time-evolving graph is preserved in the new space.
- We apply our method to real-world microbiome data to simplify the analysis of microbiome dynamics. This enables us to differentiate healthy and diseased states.
- We also analyse the low-dimensional representation of the time-evolving graph throughout visualization and comparative analysis on the clustering task, where we show that our model outperforms other unsupervised graph representation learning methods.
- We advance our research by interpreting the final low-dimensional representation learned by the model. We find topological patterns of the time-evolving graph that make the largest impact on the model decision-making. These patterns can potentially identify a set of microbes that drive microbiome constitution to undergo transitions from one metastable state to others.

2. Related work

We can broadly categorize methods for graph representation learning into semi-supervised or unsupervised methods and methods for static or time-evolving (dynamic) graphs. A good overview of the current state of methods for time-evolving and for static graph representation techniques can be found in [20, 2] and in [9, 38], respectively.

Static graph representation. Representation approaches for static graphs can be classified into two categories – those which learn the representation of nodes and those which learn the representation of sub-structures of the graphs. The first category tends to encode nodes of the graph in a low-dimensional space such that their topological properties are reflected in the new space (node2vec [16], DeepWalk[28]). Most studies are focused on node representation learning, and only a few learn the representation of the whole graph (graph2vec [26]).

Dynamic graph representation. Representing time-evolving graph in the low-dimensional space is an emerging topic that is still being investigated. Among recent approaches, DynGEM [14] uses the learned representation from the previous time step to initialize the current time step representation. Such initialization keeps the representation at the current time step close to the learned representation at the previous time step. The extension of the previous method is dyngraph2vec [15], where authors have made it possible

to choose the number of previous time steps that are used to learn the representation at the next time step. Moreover, dyngraph2vec uses recurrent layers to learn the temporal transitions in the graph. Unlike this method, we utilize the multi-head attention mechanism [35] to capture the temporal changes in the time-evolving graph.

Recently, attention-based methods have been extensively proposed, and one of them is DynSAT ([29]) that learns a dynamic node representation by considering topological structure (neighbourhood) and historical representations following the self-attention mechanism. The model is similar to our method in the way that they also use the self-attention mechanism and historical representation. However, their key focus is to learn dynamic node representation, whereas our goal is to obtain the low-dimensional representation of the entire time-evolving graph, while maintaining a dynamical property such as metastability.

However, one of the disadvantages of these methods for our problem is that time-evolving graphs with metastability usually consist of many time steps, and it is crucial to have a computationally efficient method in order to learn a low-dimensional representation. Another disadvantage is that all these methods capture the dynamic of nodes and, as the result, output the low-dimensional representation of nodes.

3. Definitions and problem statement

We first briefly introduce all necessary notations and definitions, which are used in the paper, and state the problem.

Definitions. A graph G is a pair (V, E) with a non-empty set of nodes $V(G)$ and a set of edges $E(G) = \{(v_i, v_j) \mid v_i, v_j \in V\}$. The set $V(G)$ often represents the objects in the data and $E(G)$ the relations between objects. We define the *adjacency matrix* of the graph G as the $n \times n$ matrix A with $A^{ij} = 1$ if the edge $(v_i, v_j) \in E(G)$, and 0 otherwise, where $n = |V|$.

Next, we define a metastability property, which was first mentioned in [22]. Consider a time-evolving graph \mathbb{G} as a sequence of graphs $\mathbb{G} = (G_1, \dots, G_T)$ at consecutive time points $\{1, \dots, T\}$ for some $T \in \mathbb{N}$, and G_t being a time-snapshot of \mathbb{G} at time t . The time-evolving graph \mathbb{G} exhibits *metastable* behavior if \mathbb{G} can be partitioned into s subsets $\mathbb{G} = \mathbb{G}_1 \cup \dots \cup \mathbb{G}_s$ for some $s \ll T$ such that for each time point $t \in \{1, \dots, T\}$ and $i, j = 1, \dots, s$, we have the following:

$$\begin{cases} P(G_{t+1} \in \mathbb{G}_i \mid G_t \in \mathbb{G}_j) \ll 1, & \text{if } i \neq j \\ P(G_{t+1} \in \mathbb{G}_i \mid G_t \in \mathbb{G}_j) \approx 1, & \text{if } i = j, \end{cases} \quad (1)$$

where $P(\cdot)$ is a transition probability, and $\mathbb{G}_1, \dots, \mathbb{G}_s$ are called metastable states of the time-evolving graph \mathbb{G} , where s is the number of states.

Problem statement. We define our problem as follows: *Given a time-evolving graph $\mathbb{G} = (G_1, \dots, G_T)$ with assumed metastability property (1), we aim to represent each time-snapshot G_t as a vector in a low-dimensional space*

\mathbb{R}^d , maintaining the metastable behaviour of \mathbb{G} , where d is a number of dimensions of the reduced space.

4. Proposed Method

In this section, we describe how we train the model to embed time-snapshot graphs into a low-dimensional space, maintaining the metastable behaviour of the graph. We first use the Transformer [35] to compute the embedding of a time-snapshot graph. Further, we add a recurrent mechanism to the Transformer that facilitates the learning of temporal changes across consecutive time-snapshot graphs. Finally, we use contrastive learning to make representations of consecutive time-snapshots graphs, which share metastable behaviour, close.

4.1. Transformer

The Transformer is currently the state-of-the-art method in the field of NLP, where it has shown tremendous success for handling long-term sequential data. Recently, it has become a leading tool in other domains such as computer vision [10] and graph representation learning [36, 11]. We use the encoder part of the Transformer to learn node embeddings in each time-snapshot graph. The encoder has several stacked multi-head attention layers followed by a feed-forward layer. There is a residual connection around each of these two sub-layers that is also followed by a normalization layer.

Intuitively, the self-attention in time-snapshot graphs relates different nodes of the graph in order to compute a new representation of every node in the graph to which we refer as a node embedding.

4.2. Input

Let $\mathbb{G} = \{G_1, \dots, G_T\}$ be a time-evolving graph with node features $\{x_t^v\}_{v \in V(G_t)}$, $t = 1, \dots, T$. The input node features of each time-snapshot graph G_t are embedded to d_m -dimensional latent features via a linear projection and added to pre-computed node positional encodings. In Section 6, we demonstrate on two synthetic datasets with different topological structures that our model performs well in both cases: with positional information of nodes and without it. Moreover, in order to capture the topological structure of a single time-snapshot graph G_t , we feed an adjacency matrix A_t to the Transformer as a mask, and we set attention weights to 0 whenever the corresponding adjacency matrix entries are 0.

4.3. Model architecture

In this section, we explain important details of the training of our model. The overall idea of our model can be found in Figure 1.

Let $\mathcal{T} = \{t_k\}_{k=1}^N$ be a set of randomly sampled time points, and $\mathbb{G}_{\mathcal{T}} = \{G_{t_1}, \dots, G_{t_N}\}$ be a mini-batch of time-snapshots graphs sampled from \mathbb{G} . To facilitate the learning of temporal changes, we share the embedding of a time-snapshot graph with the consecutive time-snapshot graph in the temporal sequence. We define a master node that is

Algorithm 1: Main learning algorithm

Input:

- l : the number of historical representations;
- $\mathbb{G} = \{G_1, \dots, G_T\}$: a time-evolving graph such that each time-snapshot graph $G_t = (x_t, A_t)$;
- \mathbf{z}_{init} : a randomly initialized learnable master node;
- \mathcal{R} : the Transformer
- $W, W^{(1)}, W^{(2)}, b$: parameters of the model

```

 $\mathcal{L} = 0$ ; for sampled mini batch of indices  $\{t_k\}_{k=1}^N$  do
   $\mathcal{L} = 0$ ;  $\mathbf{z}_{curr} = \mathbf{z}_{init}$ ;  $\mathbf{z}_{next} = \mathbf{z}_{init}$ 
  for  $j = 1$  to  $l$  do
    #time-snapshot graphs at time t
    Select time-snapshot graphs  $\{G_{t_k+j}\}_{k=1}^N$ 
     $\mathbf{z}_{curr} = \mathcal{R}(\mathbf{z}_{curr}, x_{t_k+j}, A_{t_k+j})$ 
    #time-snapshot graphs at time t+1
    Select time-snapshot graphs  $\{G_{(t_k+1)+j}\}_{k=1}^N$ 
     $\mathbf{z}_{next} = \mathcal{R}(\mathbf{z}_{next}, x_{(t_k+1)+j}, A_{(t_k+1)+j})$ 
    #final graph embeddings
     $\hat{\mathbf{g}}_{curr} = W\mathbf{z}_{curr} + b$ 
     $\hat{\mathbf{g}}_{next} = W\mathbf{z}_{next} + b$ 
    #projection for contrastive learning
     $\mathbf{g}_{curr} = W^{(2)}\sigma(W^{(1)}\hat{\mathbf{g}}_{curr})$ 
     $\mathbf{g}_{next} = W^{(2)}\sigma(W^{(1)}\hat{\mathbf{g}}_{next})$ 
    #pairwise similarity
     $sim = \frac{\mathbf{g}_{curr}^T \mathbf{g}_{next}}{\|\mathbf{g}_{curr}\| \cdot \|\mathbf{g}_{next}\|}$ 
     $\mathcal{L} = \mathcal{L} + \sum_{i=1}^N -\log \left( \frac{\exp(sim_{i,i}/\tau)}{\sum_{j=0}^N \exp(sim_{i,j}/\tau)} \right)$ 
  end
end
return  $\mathcal{L}$ 

```

connected to all nodes in the time-snapshot graph. Initially, the master node is represented as a learnable, randomly initialized vector. The Transformer computes the embedding of the master node which we consider as a graph embedding. This graph embedding is then passed as the initial master node to the consecutive time-snapshot graph in the temporal sequence. We control the length of temporal sequence with the hyperparameter l . Moreover, since we connect the master node with all other nodes in each time-snapshot graph, the size of the adjacency matrix changes, $A_t \in \mathbb{R}^{(n+1) \times (n+1)}$.

Formally, we update the graph embedding z_t of the time-snapshot graph G_t recursively as follows:

$$z_t = \mathcal{R}(z_{t-1}, x_t, A_t),$$

where \mathcal{R} is the Transformer that updates node embeddings discussed, $z_t \in \mathbb{R}^{d_m}$ is a master node, x_t is a vector of node features, and $A_t \in \mathbb{R}^{(n+1) \times (n+1)}$ is an adjacency matrix of G_t .

Finally, we project the graph embedding $z_t \in \mathbb{R}^{d_m}$ of the time-snapshot graph G_t into the space with the dimension d , where a downstream task is defined. We denote the final embedding of the time-snapshot graph with $\hat{g}_t \in \mathbb{R}^d$:

$$\hat{g}_t = W z_t + b$$

with W and b being learnable parameters.

We use two hidden layers and a non-linear activation function in order to project the graph embedding \hat{g}_t into the space, where the contrastive learning is defined, as it is done in [8]:

$$g_t = W^{(2)} \sigma(W^{(1)} \hat{g}_t),$$

where $W^{(1)}$, $W^{(2)}$ are learnable parameters, $\hat{g}_t \in \mathbb{R}^{d_m}$, $g_t \in \mathbb{R}^{\frac{d_m}{2}}$.

Furthermore, we explain how we use the contrastive learning to make embeddings of consecutive time-snapshots graphs preserve the metastable behaviour in the low-dimensional space.

4.4. Contrastive learning

Intuitively, contrastive representation learning can be considered as learning by comparing. Thus, the goal is to find a low-dimensional space where samples from the same instance are pulled closer and samples from different instances are pushed apart. Formally, given a vector of input samples $x_i, i = 1, \dots, N$ with a corresponding labels $y_i \in \{1, \dots, C\}$ among C classes, contrastive learning aims to learn a function $f_\theta(x)$ that can find the low-dimensional representation of x such that examples from the same class have similar representations and samples from different classes are far away from each other in a new space. One always needs to have negative and positive samples to apply contrastive learning. For this reason, we make the following assumption.

Assumption. According to the definition of metastability (1), the probability of two consecutive time-snapshot graphs G_t and G_{t+1} being similar is almost 1 and so should be the probability for their graph embeddings \hat{g}_t and \hat{g}_{t+1} .

In other words, we consider a pair of graph embeddings $(\hat{g}_t, \hat{g}_{t+1})$ as a positive pair and pairs $(\hat{g}_t, \hat{g}_{t+\tau}), t + \tau \in \{2, \dots, N\}$ as negative pairs, where τ is randomly sampled. It is feasible for negative samples to be of the same metastable states, but at different time points.

Given graph embeddings g_t and g_{t+1} for G_t and G_{t+1} as the output of our model, we first compute the similarity between g_t and g_{t+1} :

$$sim_{t,t+1} = \frac{g_t^T \cdot g_{t+1}}{\|g_t\| \cdot \|g_{t+1}\|}.$$

With the above assumption, diagonal elements of sim represent positive pairs and off-diagonal elements negative pairs. Then, the similarity score is fed to the Noise Contrastive Estimator (NCE) loss:

$$\mathcal{L} = -\log \left(\frac{\exp(sim_{t,t+1}/\tau)}{\sum_{j=1}^T \exp(sim_{t,j}/\tau)} \right).$$

Minimizing this loss function forces the parameters of the model to be tuned such that graph embeddings of two consecutive time-snapshot graphs is as close as possible.

4.5. Positional Encoding

Most graph neural networks learn structural node information that is invariant to the node positions. However, there are cases when topological information is not enough. To demonstrate this, we conduct experiments on two different synthetic datasets. The first data has metastable states with defined graph features that can be distinguished only with the position information of nodes. Each metastable state in the second data has specific graph features, which are easily distinguished with just topological information.

To incorporate the positional information, we use the same positional encoding as in [13]:

$$p_{pos,2i} = \sin pos / 10000^{2i/d_m}$$

$$p_{pos,2i+1} = \cos pos / 10000^{2i/d_m},$$

where pos , i and d_m denote a position of the node in the time-snapshot graph, the dimension in the positional encoding and the dimension of node embedding, respectively.

Through a set of various experiments in the next section, we demonstrate on synthetic and real-world datasets that our method is capable of learning a graph embedding of the time-evolving graph.

5. Datasets

Here, we briefly describe the datasets which are used to evaluate our model. Besides experiments with synthetic datasets, we also show the application of our method to real-world microbiome data. Both the whole idea of generating synthetic dataset and the idea of pre-processing real-world datasets are explained in more details in [22]. We will just briefly explain some details below. An overview of the used datasets is shown in Table 1.

5.1. Synthetic data

To assess the proposed method, we generate synthetic datasets with both understandable topological structures and temporal patterns. We use the following Stochastic Differential Equation (SDE) to sample a trajectory based on which time-snapshot graphs $\{G_1, \dots, G_T\}$ are built:

$$dX_t = -\nabla F(X_t)dt + \sqrt{2\beta^{-1}}dW_t \quad (2)$$

with the potential function:

$$F(x) = \cos(s \arctan(x_2, x_1)) + 10 \left(\sqrt{x_1^2 + x_2^2} - 1 \right)^2, \quad (3)$$

where s is the number of states or wells, $X_t = (x_t^1, x_t^2)$, W_t is a standard Wiener process, β is the inverse temperature that controls the transition between states. The higher β , the less likely is the transition from one state to another. We use this potential function to generate pos_3WellGraph.

Table 1
Statistics of each dataset used in this paper.

Name	# Nodes	# Edges (avg.)	# Time steps	# States
npos_2WellGraph	150	10821	10000	2
pos_2WellGraph	100	4109	10000	2
pos_3WellGraph	150	10869	10000	3
CholeraInf	96	106	34	2
MovingPic	919	10602	658	2

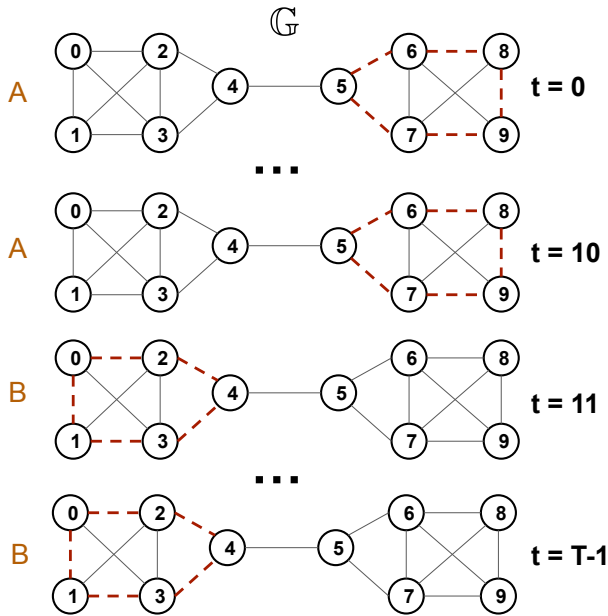


Figure 2: The example of a time-evolving graph with metastability whose two states A and B are difficult to distinguish since they are topologically the same. Red dashed edges are removed from the time-evolving graph \mathbb{G} .

For the synthetic datasets with 2 states (pos_2WellGraph and npos_2WellGraph), we use the following potential function, which is often called the double-well potential:

$$F(x) = \frac{x^4}{4} - \frac{x^2}{2}, \quad (4)$$

where $X_t = x_1$.

We further split our synthetic datasets into two categories: positional and non-positional data. Positional data means that we use the positional encoding explained in Section 4 before training the model, since the structure of the data does not allow learning the graph embedding without this information. Non-positional data means the opposite – we do not use the positional encoding, as the topological structure of the time-evolving graph can be understood without providing the positional information of the node. We define these two categories to show that our model does not rely on the positions of nodes if the topological patterns differentiating states are clearly defined.

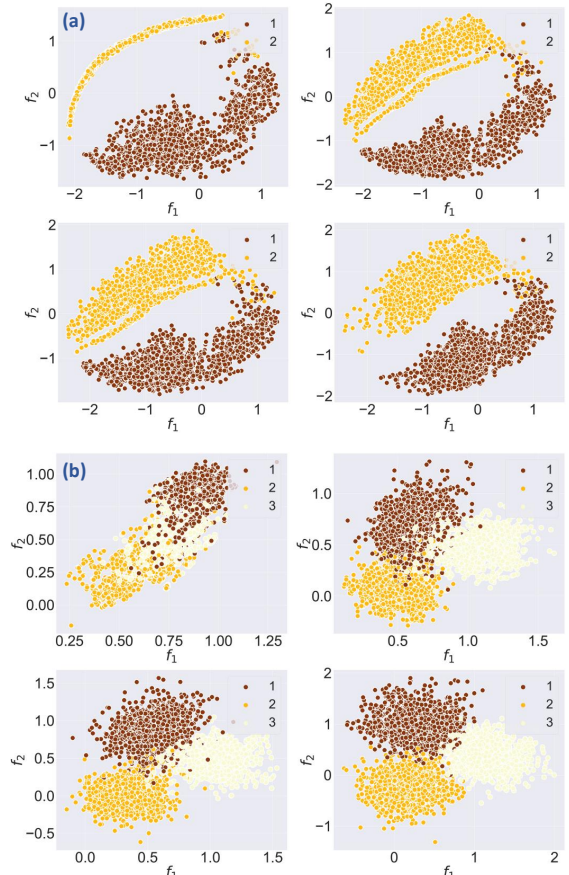


Figure 3: The evolution of the graph embedding of the time-evolving graph \mathbb{G} during the training of our model on synthetic datasets: (a) npos_2WellGraph and (b) pos_3WellGraph. The points are coloured according to ground-truth labels.

Positional data. This synthetic data has a topological structure that is difficult to distinguish without the positions of nodes. We briefly describe the three-step process, which generates the positional time-evolving graph:

- We sample the trajectory $S = \{(x_1^{(i)}, x_2^{(i)})\}_{i=1}^T$ using SDE (2), and the corresponding potential function (3) or (4).
- Then we choose the number of nodes n , and assign random coordinates $(a_j, b_j), j = 1, \dots, n$ to each of these nodes. The reason for that is to be aware of the locations of discriminating features of metastable states.

- In the final step, we define discriminating topological features for each state. Let G_0 be a complete graph. In case of the s -well potential, we generate G_t , $\forall t, t = 1, \dots, T$ by drawing a circle with the centre at (x_1^t, x_2^t) and the radius r and removing edges with a probability between nodes that are inside the current circle. In addition, to address the noise in the real-world data, we randomly remove edges outside the current circle. For double-well potential, we remove edges between nodes, which satisfy $b_j > \frac{1}{T} \sum_{i=1}^T x_1^i$.

We can see that the graph features of different states are the same for the model, and it result in that the model will fail to discriminate between metastable states in the time-evolving graph. As an illustration of that, we provide Figure 2. There we have two states A and B of the time-evolving graph \mathbb{G} that are characterized by removed edges in the right part of \mathbb{G} for the state A and in the left part of the graph for state B . Topologically, states have the same neighbourhood structure, which will result in the same point in the low-dimensional space. The same occurs for our synthetic dataset: nodes in the circles determine metastable states, and neighborhoods of these nodes are almost identical for the model.

Non-positional data. This type of data has a dissimilar topological pattern to the positional data. The time-evolving graph is generated in the same way as the positional synthetic dataset, except instead of removing a random number of edges between nodes that fall in the circle, we remove edges between nodes in the circle in such a way that each node does not lose the particular number of neighbours. We define the number of removed neighbors of nodes arbitrary and different for each state. In this case, nodes in each state have a specific number of lost neighbours, which makes metastable states have completely different topological patterns.

5.2. Real-world dataset

MovingPic. This dataset, originally introduced in [3], is the first real-world dataset on which we evaluate our model. In this study, one male and one female were sampled daily at three body sites (gut, skin, and mouth) for 15 months and for 6 months, respectively. To obtain a time-evolving graph, we pre-process Operational Taxonomic Units (OTU) that contains the number of 16S rDNA marker gene sequences that are observed for each taxonomic unit in each sample. Let $D \in \mathbb{R}^{T \times p}$ be an OTU table, where T is the number of time points and p is the number of OTUs. As this data does not have any obvious perturbations, such as antibiotics exposure or diseases, which could potentially create a metastable structure, an artificial noisy signal is added to the data. The Pearson correlation between two OTUs is computed, and then the initial time-snapshot graph is constructed. To construct time-snapshot graphs at each time step, the authors of [22] use the OTU table to remove edges between nodes. If the OTU count for a particular node is zero, then the edge is removed between this node and its neighboring nodes.

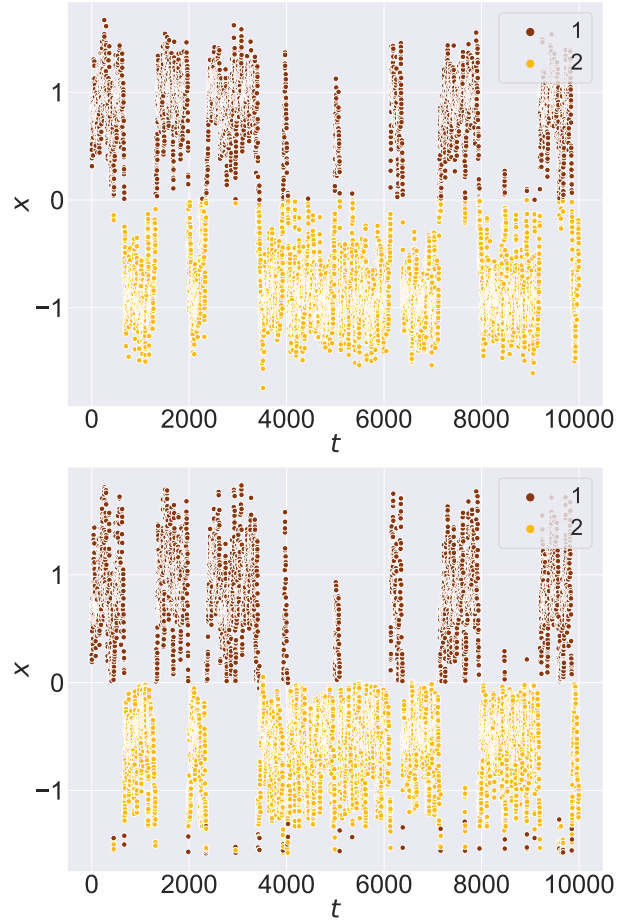


Figure 4: Trajectories of *npos_2WellGraph*. **Top:** The trajectory sampled from SDE (2) with the potential function (4), which is used to construct the time-evolving graph. **Bottom:** The graph embedding obtained by our model.

CholeraInf. This dataset has been introduced in a study about the recovery from *Vibrio Cholera* infection [17]. Here, faecal microbiota were collected from seven cholera patients from disease (state 1) through recovery (state 2) periods. Moreover, in our experiment, we use the microbiome of one patient, since the variation in the microbiome constitution among individuals can have an impact on the result of the model. The time-evolving graph is obtained in the same way as it has been done for the MovingPic dataset.

6. Experiments and Results

In this section, we evaluate our method proposed in Section 4 by primarily analysing the graph embedding on different datasets, then we demonstrate how efficient our method is in comparison with other methods in the field of graph representation learning on a downstream task such as clustering of time-snapshot graphs. In the end, we take our study forward by incorporating an interpretation method in order to investigate whether the model uses the topological structure, which we have defined as discriminating features of metastable states. Furthermore, such analysis can also

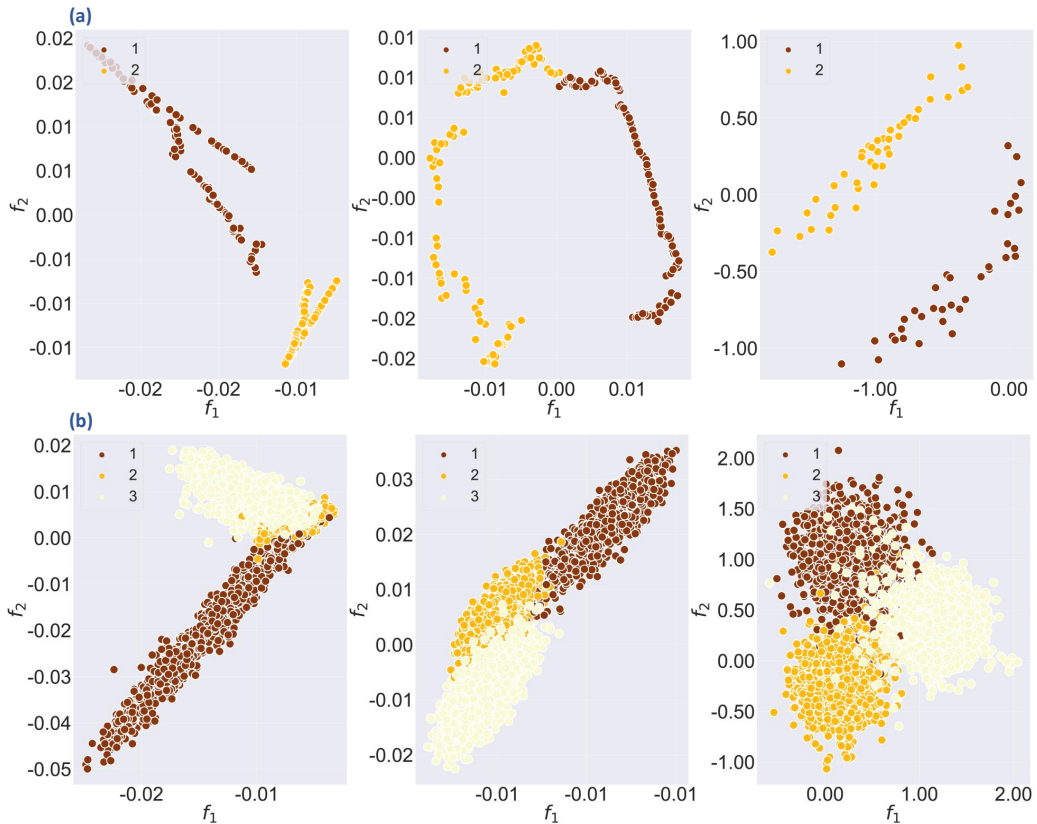


Figure 5: The graph embedding of the time-evolving graph for synthetic datasets: (a) npos_2WellGraph and (b) pos_3WellGraph. From left to right: PCA on adjacency matrices, PCA on eigenfunctions of graphKKE and the result of our method. The points are coloured according to ground-truth labels.

reveal additional information in microbiome data that can be utilized to improve the treatment of different diseases.

6.1. Analysis of graph embedding

In this part of the paper, we concentrate on the analysis of the graph embeddings on both synthetic and real-world datasets. Our model is compared to the following methods: a simple baseline chosen from state-of-the-art methods for dimensional reduction, namely, **Principal Component Analysis (PCA)**, two kernel-based methods **graphKKE** [22] and **WL kernel** [31], and two graph representation learning methods **node2vec** [16], and **graph2vec** [26]. We evaluate our method and other baselines by visualizing the graph embedding and clustering points of the final representation.

- Principal Component Analysis (PCA) is a method for dimensional reduction. To be able to apply this method to the time-evolving graph, we flatten an adjacency matrix of each time-snapshot graph into a vector.
- The graphKKE approach is exclusively proposed for learning the embedding of a time-evolving graph with assumed metastability. It is a graph kernel-based method that combines a transfer operator theory and a graph kernel technique, namely, the Weisfeiler–Lehman (WL) kernel.

- The WL kernel decomposes graphs into rooted subgraphs using a specific relabelling process and computes feature vectors based on the number of initial and updated labels.
- The graph2vec approach projects the set of static graphs, and it comprises two main components: 1) Weisfeiler–Lehman relabeling process and 2) the Skip-gram procedure from doc2vec.
- The node2vec algorithm is a node representation method that uses breadth-first search and depth-first search to extract local and global information from the static graph.

Evaluation metric. In order to measure the performance of our method and compare the result to other methods, we use a standard clustering evaluation metric, namely, the Adjusted Rand Index(ARI). The ARI values lie in the range $[-1; 1]$ with 0 representing random clustering and 1 being the highest correspondence to the ground-truth data.

Experimental setup. First, we examine the evolution of the graph embedding by visualizing it at the beginning, in the middle and at the end of the training for npos_2WellGraph, pos_3WellGraph, MovingPic and CholeraInf. To do so, we use the low-dimensional vector $\hat{g} = \{\hat{g}_1, \dots, \hat{g}_T\}$, where $\hat{g}_i \in \mathbb{R}^d$ with $d = 2$. For all synthetic datasets, we set the

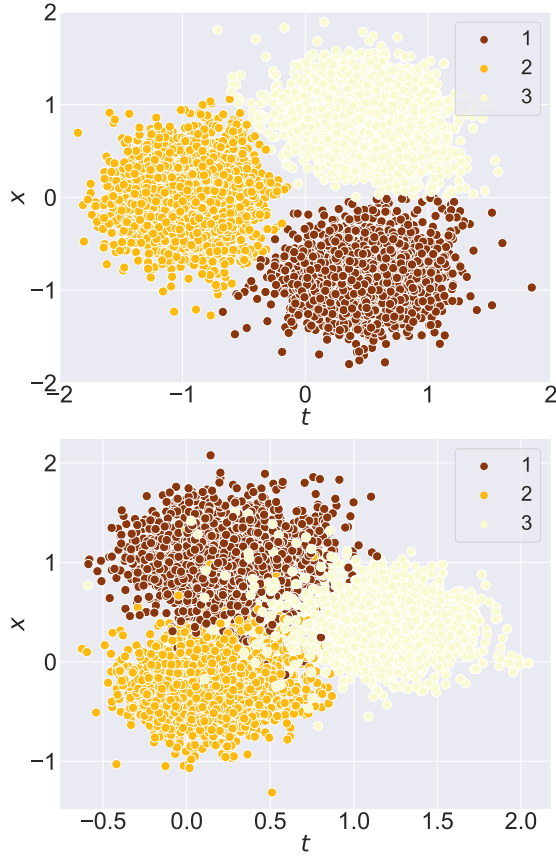


Figure 6: Trajectories of *pos_3WellGraph*. **Top:** The trajectory sampled from SDE (2) with the potential function (3), which is used to construct the time-evolving graph. **Bottom:** The graph embedding obtained by our model.

hyperparameter l to be 3, the number of epochs to be 200 for *pos_3WellGraph* and 1000 for *npos_2WellGraph*. For real-world data, the batch size is set to be 64 for *MovingPic* and 6 for *CholeraInf*. We use the Adam optimizer with default parameters, the number of heads of the Transformer 4 and the number of layers in the Transformer 3.

Furthermore, we are interested whether metastable states of the original space correspond to the clusters of points in the reduced space, so we colour points in the reduced space with original ground truth states.

As the graphKKE method approximates the eigenfunctions of a transfer operator, the dimension of the graph embedding equals the number of metastable states in the time-evolving graph. This means, we need to apply a dimensional reduction method to be able to visualize it. Thus, PCA is also applied to the output of graphKKE with the number of components to be two.

We set a number of dimensions of graph embeddings to be 32 for our method, node2vec, graph2vec and PCA. We use author-provided implementations for node2vec and graph2vec with the default hyperparameters. GraphKKE has the number of dimensions of the representation to equal to the number of metastable states in the time-evolving graph.

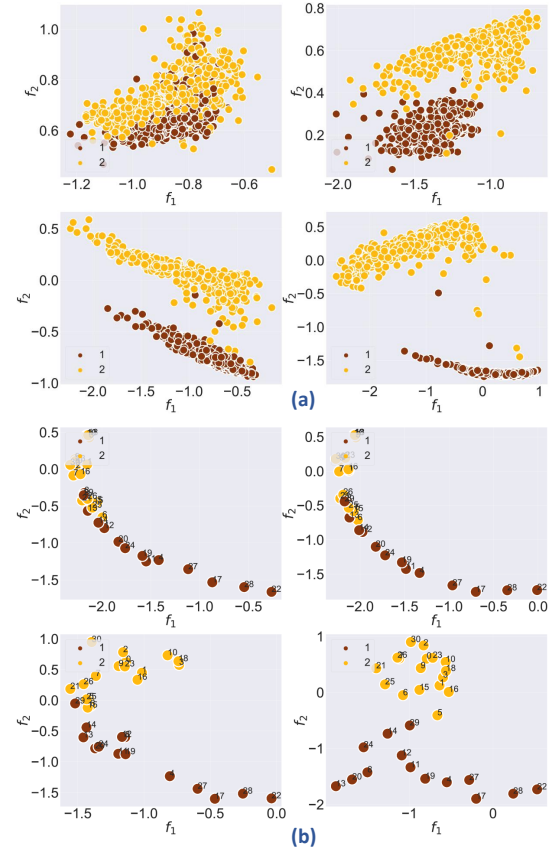


Figure 7: The evolution of the graph embedding of the time-evolving graph \mathbb{G} during the training of our model on (a) *MovingPic* and (b) *CholeraInf*. The points are coloured according to ground-truth labels.

We apply k -means to cluster points of final representations resulted from each method. Since node2vec is developed to learn node representations, we average the graph embedding to obtain representations of entire time-snapshot graphs.

Results and Discussion: Synthetic data. The evaluation of the graph embedding for both synthetic datasets — *npos_2WellGraph* and *pos_3WellGraph* — are illustrated in Figure 3. The visualization demonstrates that during the training, our model tends to capture the underlying metastable structure in the time-evolving graph. Moreover, at the end of the training, we see that our method is able to learn the graph embedding maintaining the initial metastable dynamics. Although in the case of the *npos_2WellGraph* dataset, there is no obvious split between the two classes, this is because the initial SDE trajectory has points that are located on the boundary between two states. On Table 2, we can see that these results are reinforced by the high ARI values for our methods. This result also demonstrates that graphKKE outperforms our method and all other methods. However, if we look at the visualization of the graph embedding obtained with graphKKE (Figure 5), we see that graphKKE+PCA fails to produce a visualization with clear states. This is one of the disadvantages of this method, since

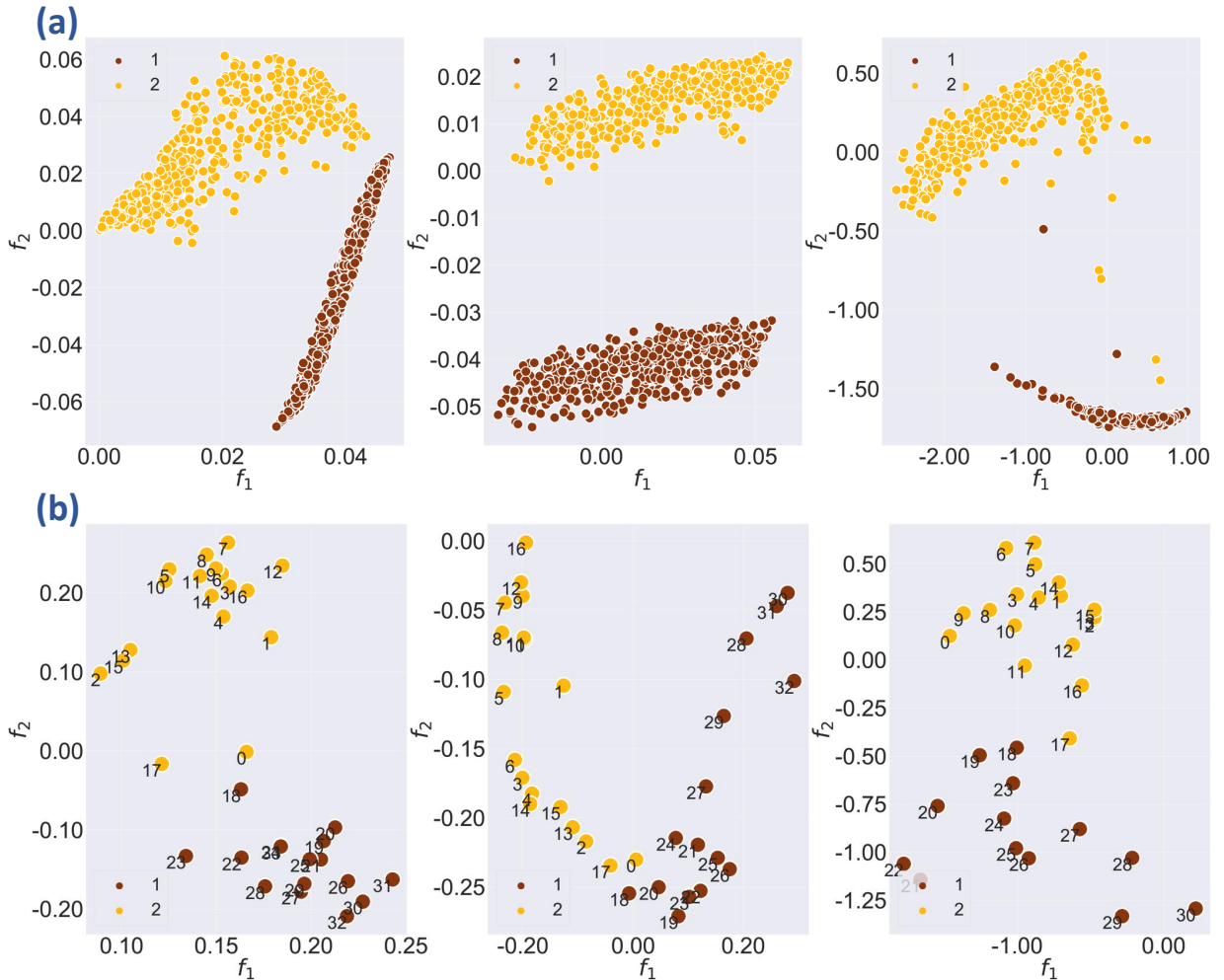


Figure 8: The graph embeddings of the time-evolving graph \mathbb{G} for (a) MovingPic and (b) CholeraInf. From left to right: PCA on adjacency matrices, PCA on eigenfunctions of graphKKE and the result of our method.

it does not allow to select a preferable number of dimensions for the representation. Thus, we apply PCA to flattened adjacency matrices, which gives us the same visualization result as graphKKE.

Moreover, considering the results of graph representation learning (Table 2), node2vec fails completely to learn the graph embedding of the time-evolving graph and graph2vec performs poorly on all synthetic datasets except npos_2WellGraph. This is because graph2vec struggles to identify states in the positional data because states do not have unique topological patterns.

Furthermore, we compare the initial SDE trajectory and the final graph embedding with $d = 1$ for npos_2WellGraph and with $d = 2$ for pos_3WellGraph. The result for npos_2WellGraph is presented in Figure 4 which shows that two trajectories are almost identical. The same result can be seen for pos_3WellGraph in Figure 6. These results indicate that the model is capable of extracting the underlying metastable dynamics in the time-evolving graph.

Result and Discussion: Real-world data. In the case of real-world datasets, the evaluation of the low-dimensional

representation for MovingPic and CholeraInf are presented in Figure 7. As it was in the case of synthetic datasets, our method is also able to identify the metastable behaviour in the time-evolving graph and maintain it in the new space. For CholeraInf we have added time-points from the original dataset to see if the new space has the same time order as it was in the original high-dimensional space.

The second part of this experiment aims at comparing our model with other dimensional reduction methods at learning the graph embedding. The results are shown in Figure 8 for both datasets. It is apparent that all methods have managed to detect two states in both real-world datasets and, consequently, to learn the graph embedding which has the same metastable behaviour as the time-evolving graph. If we have a closer look at the result for the CholeraInf dataset, we can notice that only our method retains consecutive time points in the new space.

7. Opening a black box

An improved understanding of how the microbiome contributes to health and well-being can drive and accelerate

Table 2

Adjusted Rand Index (ARI) for the comparative analysis on the graph clustering task. ARI close to 1 corresponds to greater accuracy in correctly identifying the ground truth states, and an ARI value close to 0 stands for random clustering.

Dataset	graphKKE	WL kernel	graph2vec	node2vec	our method
npos_2WellGraph	0.99	0.98	0.963	0.000	0.99
pos_2WellGraph	0.97	0.97	0.046	0.000	0.82
pos_3WellGraph	0.93	0.11	0.003	0.000	0.80
MovingPic	0.99	0.56	0.42	0.078	0.99
CholeraInf	0.88	0.66	0.29	-0.017	0.87

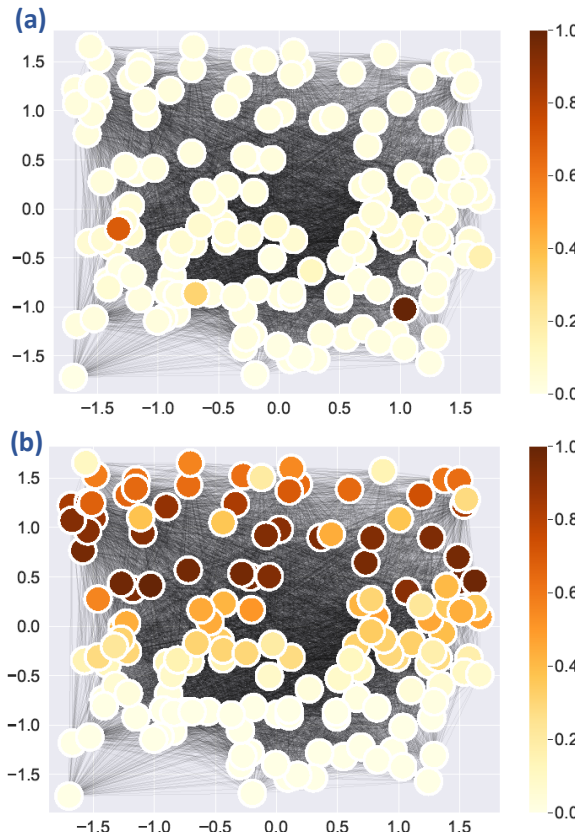


Figure 9: Fully-connected graphs for non-positional 2Well-Graph dataset with nodes coloured based on the relevance score of the LRP interpretation, which is summed across 2 states: (a) State 1 (b) State 2. The locations of 2 states are obtained by clustering points of the low-dimensional representation of the time-evolving graph via k-means.

the development of microbiome-based treatments. The most important question, which has not been answered yet, is which species or interactions of species might be responsible for or affected by the changes which the biological interaction network undergoes from one state (healthy) to another state (diseased or antibiotic exposure). The presence of such valuable information can improve modern treatments of various diseases significantly. Therefore, the main aim of this section is to provide an insight to which extent the model makes a decision based on discriminating features that we,

as humans, have added to the data. And with regard to real-world data, our objective is to obtain knowledge about which topological features make the two states, cholera infection period and recovery period, different.

We make use of two approaches: the visualization of the attention matrix and layer-wise relevance propagation (LRP) [1]. In the following section, we briefly describe the main ideas of these two approaches.

7.1. Method

LRP. Layer-wise relevance propagation (LRP) [1] is the family of explanation methods that leverages the layered structure of the network. It explains the prediction of a neural network classifier by backpropagating the neuron activation on the output layer to the previous layers until the input layer is reached. Such redistribution results in the attribution of the predictions to the different input features.

Formally, LRP can be defined in the following way. Given j and k neurons in two consecutive layers of the neural network, the relevance score at the layer l is computed in the following way:

$$R_j^{(l)} = \sum_k \frac{a_j w_{jk}}{\sum_{0,j} a_j w_{jk}} R_k^{(l+1)}, \quad (5)$$

where a_j is the activation of the neuron j , w_{jk} is a weight between neurons j and k , and $R_k^{(l+1)}$ is a relevance score of the neuron k at the $(l+1)$ -th layer.

In order to explain the output and pave the way for a better explanation of our model, we utilize the idea from [7]. The authors address the lack of the conservation property in the attention mechanism because of matrix multiplication and the numerical issues of the skip connections by applying a normalization to the computed relevance score. Moreover, they make use of the attention weights and propose to compute the final relevance scores by multiplying the relevance score of each Transformer layer with the gradient of the corresponding attention matrix summed up across the “head” dimension.

Unlike original LRP and [7], where the decomposition starts from the classifier output corresponding to the target class, we have a similarity model that rather measures how similar graph embeddings of the time-snapshot graphs G_t and G_{t+1} are. For this reason, we start the redistribution from the layer, where we have computed the graph embedding \hat{g}_t .

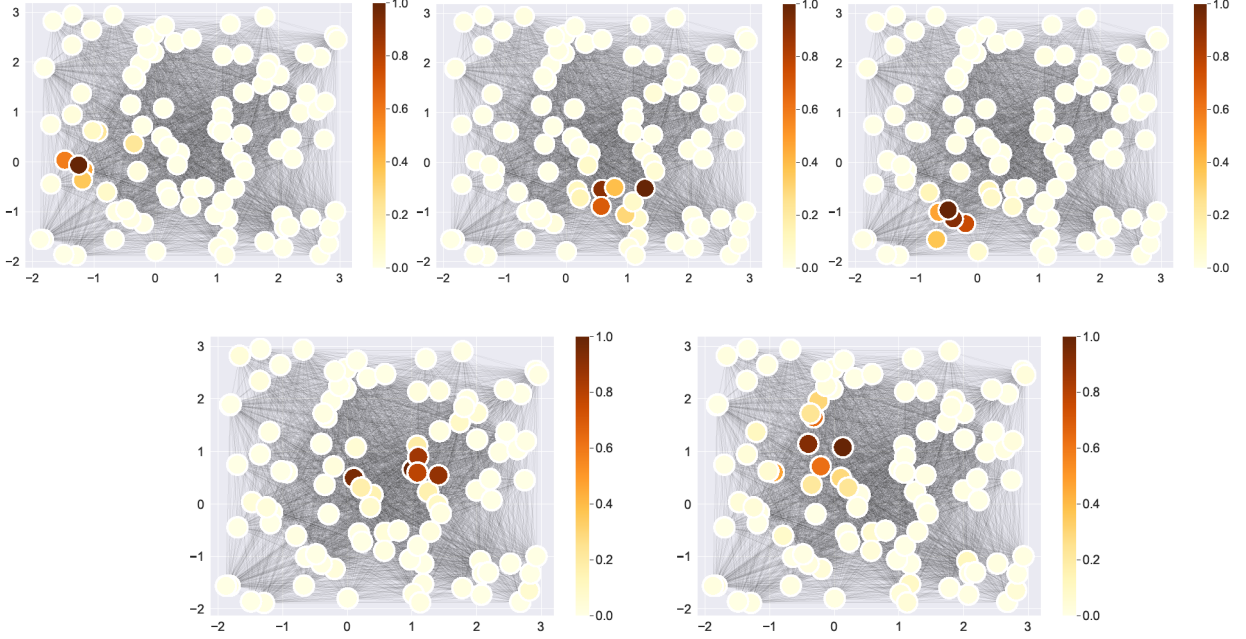


Figure 10: Fully-connected graphs for pos_5WellGraph dataset with nodes coloured based on the relevance score of the LRP interpretation, which is summed across 5 states. The locations of 5 states are obtained by clustering points of the graph embedding of the time-evolving graph via k -means.

Then we redistribute using Eq. (5) until the input layer is reached, and the final relevance $R^{(1)}$ is computed.

We compute a relevance score for each time-snapshot graph in the test set. To obtain discriminating features of the whole state, we sum up relevance scores of time-snapshot graphs of each state:

$$R_s = \frac{1}{|T_s|} \sum_{i \in T_s} R_i^{(1)},$$

where s is an index of the state, T_s is a set of indices of time-snapshot graphs from the state s , $R_i^{(1)}$ is a matrix of final relevance scores of the i -th time-snapshot graph.

Attention matrix. The attention matrix as an explanation of individual predictions has been extensively studied in [34, 18, 37, 32]. Although these works have shown through a set of experiments that the correlation between learned attention weights and feature importance is weak, we visualize the attention weights of each head in the Transformer to compare the results with LRP.

As in the case of LRP, we extract attention weights for each time-snapshot graph G_t in the test set. The sum of attention weights for each state is then computed to obtain discriminating features of the entire state. That is:

$$\hat{H}_s = \sum_{i=1}^{T_s} H_i,$$

where s is an index of the current state, $H_i \in \mathbb{R}^{(n+1) \times (n+1)}$ is an attention matrix extracted from the model with the

input of the time-snapshot G_i and T_s is the number of time-evolving graphs in the state s .

Since $\hat{H}_s \in \mathbb{R}^{(n+1) \times (n+1)}$, where the $(n+1)$ th node is the master node which we use as a graph embedding of the entire time-snapshot graph, we assume that this node encapsulates an explanation of the whole time-snapshot graph.

7.2. Experiments and Results

We infer discriminating features of the time-evolving graph, on which the model relies the most, for several synthetic datasets and real-world datasets.

Results and Discussion: Synthetic dataset. In this paragraph, we assess the interpretation results for the synthetic dataset, which was defined in Section 5.1. We use the npos_2WellGraph dataset and also, we generate a new dataset that is similar to pos_3WellGraph but with 5 metastable states. We refer to this dataset as pos_5WellGraph.

We begin with the results of the interpretation for the npos_2WellGraph dataset. The average attention matrix of each head of the multi-head attention mechanism is given in Figure 12. As it is evident from the visualization, the model's focus is on both upper and lower parts of the time-snapshot graph. These areas are also discriminating for us as humans to distinguish structural patterns of time-snapshot graphs in both states. It is interesting that the attention matrix of one state contains the information of another state, which is different in the case of LRP.

In the case of LRP for npos_2WellGraph, whose results are presented in Figure 9, the interpretation seems to be counter-intuitive. For instance, the interpretation of state 1 (Figure 9b) highlights the upper part of the time-snapshot

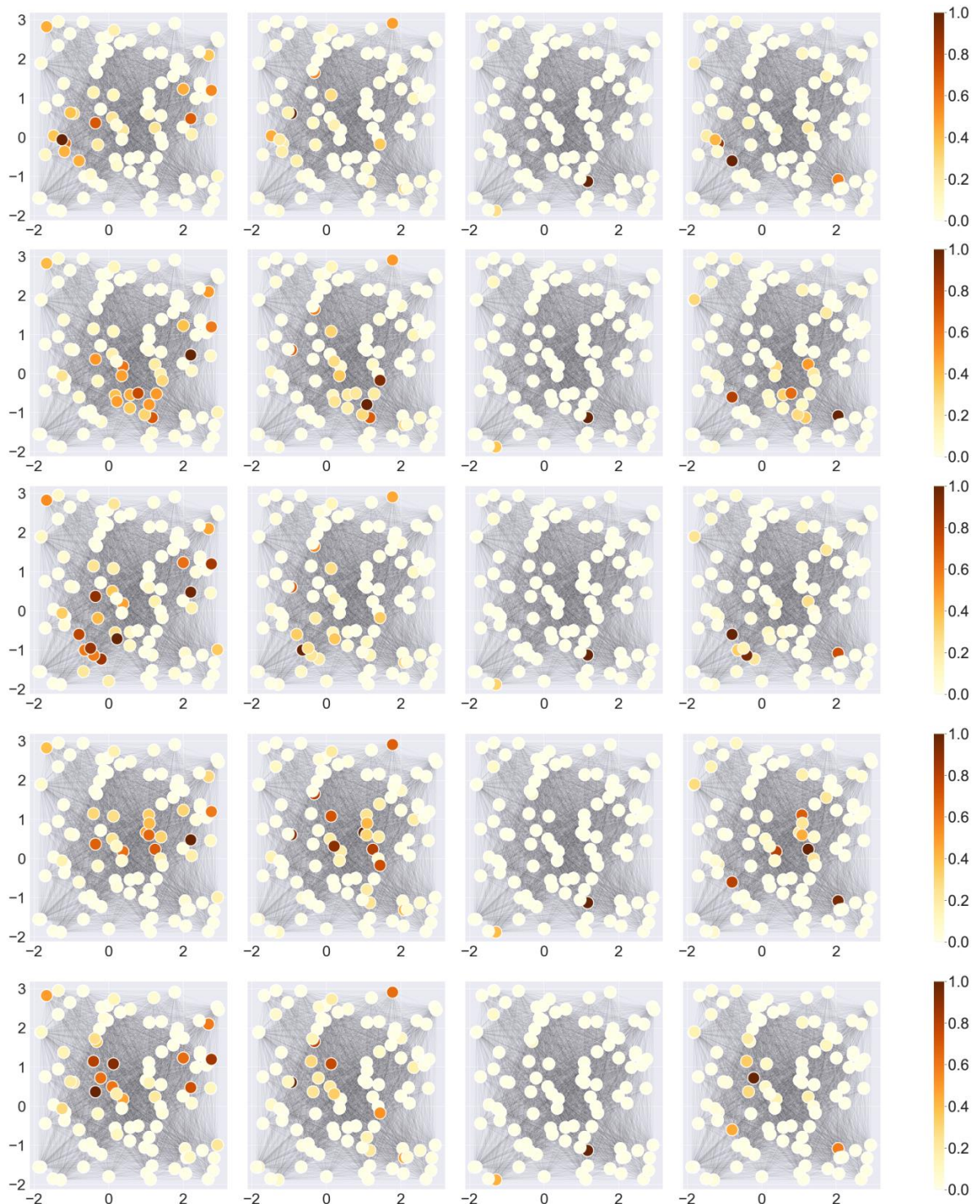


Figure 11: Fully-connected graphs for pos_5WellGraph dataset with nodes coloured based on attention weights for each of 4 heads in the Transformer, which are extracted from the model during learning the graph embedding of each time-snapshot graph and summed across states. The locations of 5 states are obtained by clustering points of the graph embedding of the time-evolving graph via k -means.

graph, which is a true discriminating feature that was defined by us, however, the interpretation of state 0 shows only 4 importance nodes in the lower part of the time-snapshot graph. This result should be investigated further since the method, which we employ here to interpret the model, uses not only relevance scores computed by the original LRP, but

also the information from attention matrices and attention weights containing the entire node cluster that we define as the discriminating feature. However, the visualizations of both approaches are slightly contradictory.

Let us examine the result of the last synthetic dataset that is pos_5WellGraph. As before, we discuss first the result of

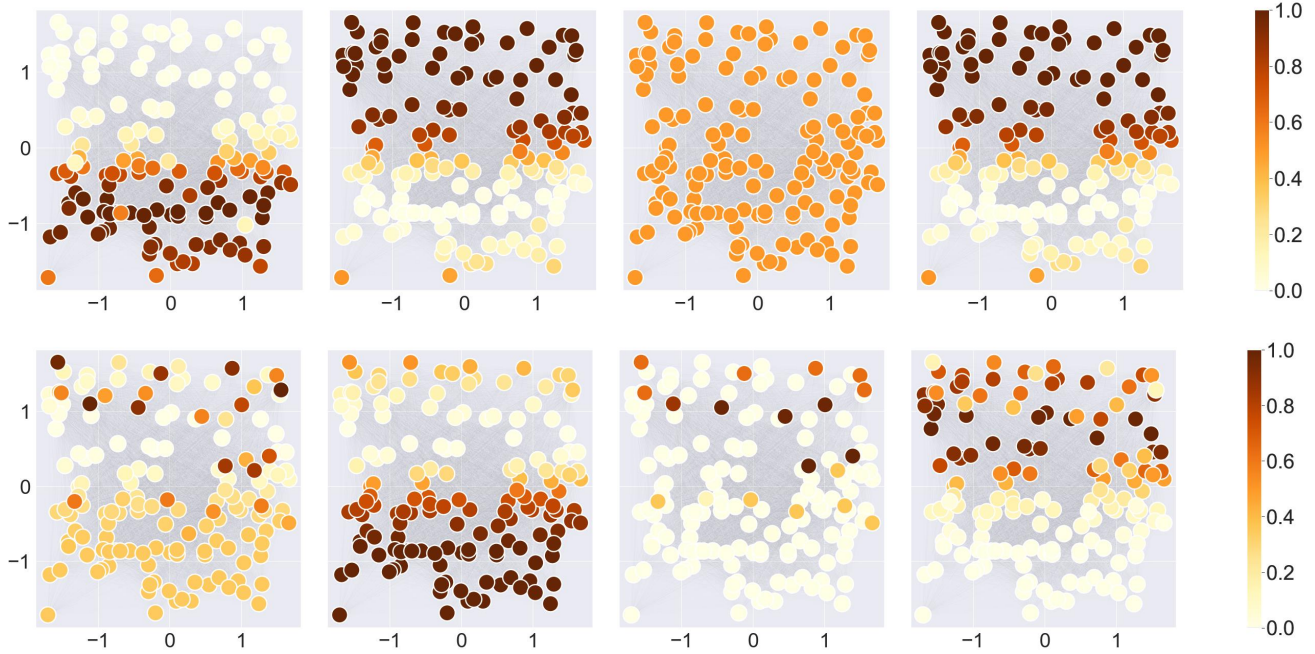


Figure 12: Fully-connected graphs for npos_2WellGraph dataset with nodes coloured based on attention weights for each of 4 heads in the Transformer, which are extracted from the model during learning the graph embedding of each time-snapshot graph and summed across 2 states. The locations of 2 states are obtained by clustering points of the graph embedding of the time-evolving graph via k -means.

visualizing attention matrices and then the result of LRP. Figure 11 shows attention matrices of 4 heads for each of 5 states. As it was with npos_2WellGraph, the visualization of attention weights shows the presence of 5 different clusters of nodes and some heads have information about the locations of discriminating features of other states as well. Unlike the LRP result for npos_2WellGraph, the interpretation for pos_5WellGraph via LRP (Figure 10) highlights clusters of nodes, which are considered as discriminating features of metastable states.

There is a necessity to mention that we have modelled these synthetic datasets in such a way that we know the location of nodes in the graph. Therefore, the visualization of interpretation results has not been difficult, but in the real-world setting we do not have coordinates of nodes and the visualization of interpretation results might be an issue. Such cases must be investigated in further work.

Results and Discussion: Real-world dataset. We have assessed the interpretation of our model on the synthetic dataset, and now we focus on obtaining the interpretation of the model’s decision for the real-world dataset, namely, CholeraInf, which has been described in Section 6. Unlike the synthetic dataset, we do not know the ground truth discriminating features for this data. Moreover, to visualize the interpretation, we use a correlation matrix that has been computed based on the OTU table (see more details about how this data has been pre-processed in [22]). We begin with the visualization of attention weights.

Figure 13 shows the interpretation assessment through the attention matrix. If we have a closer look at these plots,

we can see that the attention matrix of the first head contains the most different node clusters, while other heads’ clusters are overlapping. The question whether the model relates time-snapshots graphs based on just the first head or not needs to be investigated further.

LRP results for both metastable states are presented in Figure 14, where we have obtained two clear clusters of nodes, although there are the same nodes in both states that are significant for the model. For example, the relevance scores of node 73 and node 4 are high in both states.

Further study of these results is needed to investigate if these interpretations have biological meaning. For instance, there have been done numerous works [21] that are mainly focused on statistical analysis to justify which bacteria/species are affected by, or on the contrary, cause shifts in microbiome compositions. Using the detected species from these works, we can compare them with the nodes that have shown the biggest impact on the model output according to both the LRP approach and the visualization of attention weights.

8. Conclusion

We have presented a new approach that can simplify the analysis of time-evolving graphs with assumed metastability. Through an extensive set of experiments on both synthetic and real-world datasets, we have demonstrated that our approach is capable of projecting a time-evolving graph into a low-dimensional space retaining metastable properties of the system. Moreover, we have illustrated one of the possible applications of this approach to microbiome data

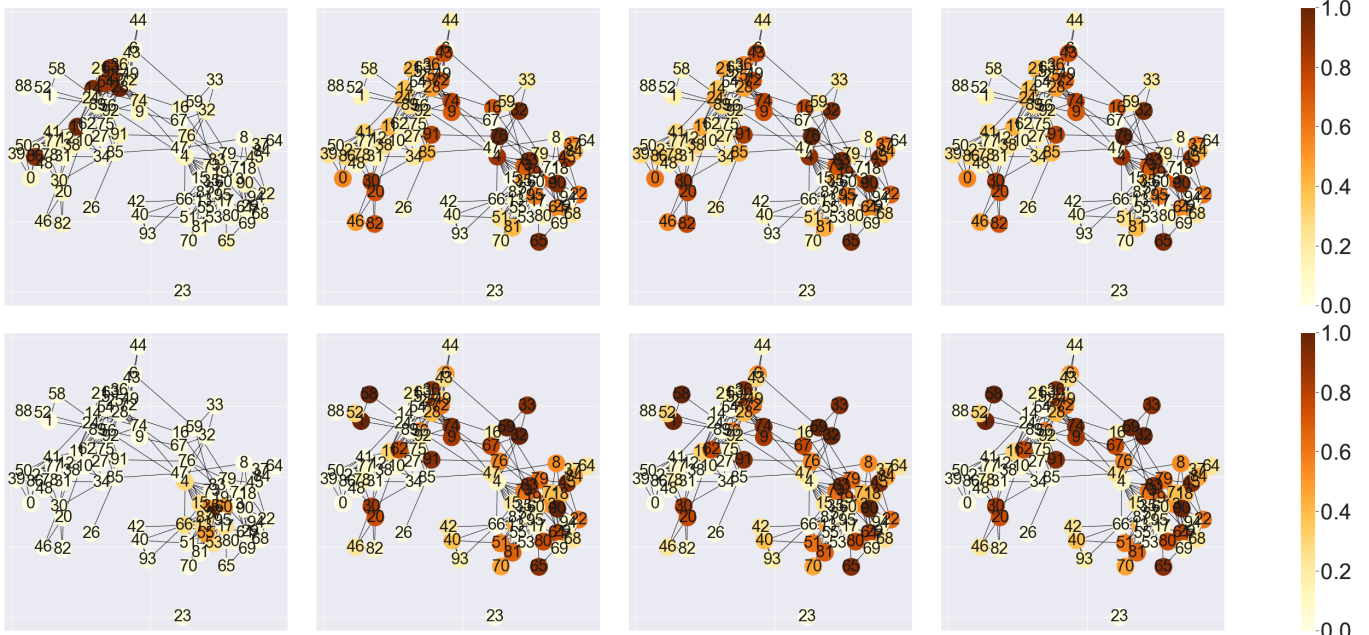


Figure 13: Co-occurrence interaction graphs of CholeraInf dataset with nodes coloured based on attention weights for each of 4 heads in the Transformer. Attention weights are extracted from the model during learning the graph embedding of graph-snapshot graphs and summed across each state. The locations of states are obtained by clustering points of the graph embedding of the time-evolving graph via k -means. The dark brown colour indicates nodes with the highest attention weights.

that enhances the analysis of metagenomic data in a way that it takes into account a huge number of interactions among species. We have shown that through explaining the output of the model, we can find topological graph features, such as nodes or edges, that make the model arrive at a certain graph embedding. Concerning microbiome data, it means that our method coupled with a proper interpretation strategy can help to reveal underlying disease patterns in the data.

There are several directions for future work: 1) how to construct a time-evolving graph from metagenomic data such that it contains a real dynamics occurring in the microbiome; 2) further biological analysis of results obtained from the interpretability of the model; 3) visualization of topological graph features, such as nodes and edges, that have impacted the model the most, and 4) mathematical explanation of how the model learns a graph embedding of the time-evolving graph maintaining metastable dynamics.

Acknowledgement

This work was supported by the Forschungscampus MODAL (project grant 3FO18501) and funded by Berlin Institute for the Foundations of Learning and Data (BIFOLD, ref. 01IS18025A and ref. 01IS18037I) and by the Deutsche Forschungsgemeinschaft (DFG, German Research Foundation) under Germany Excellence Strategy – The Berlin Mathematics Research Center MATH+ (EXC-2046/1, project ID: 390685689).

References

- [1] Bach, S., Binder, A., Montavon, G., Klauschen, F., Müller, K.R., Samek, W., 2015. On pixel-wise explanations for non-linear classifier decisions by layer-wise relevance propagation. *PLoS ONE* 10(7).
- [2] Barros, C.D.T., Mendonça, M.R.F., Vieira, A.B., Ziviani, A., 2021. A survey on embedding dynamic graphs. *ArXiv* abs/2101.01229.
- [3] Caporaso, J., Lauber, C., Costello, E., Berg-Lyons, D., Gonzalez, A., Stombaugh, J., Knights, D., Gajer, P., Ravel, J., Fierer, N., Gordon, J., Knight, R., 2011. Moving pictures of the human microbiome. *Genome biology* 12, R50. doi:10.1186/gb-2011-12-5-r50.
- [4] Chambers, L., Bussies, P., Vargas, R., Esakov, E., Tewari, S., Reizes, O., Michener, C., 2021. The microbiome and gynecologic cancer: Current evidence and future opportunities. *Current Oncology Reports* 23.
- [5] Chang, W.K., VanInsberghe, David andKelly, L., 2020. Topological analysis reveals state transitions in human gut and marine bacterial communities. *npj Biofilms and Microbiomes* 6. doi:10.1038/s41522-020-00145-9.
- [6] Chattopadhyay, I., Dhar, R., Pethusamy, K., Seethy, A. and Srivastava, T., Sah, R., Sharma, J., Karmakar, S., 2021. Exploring the role of gut microbiome in colon cancer. *Applied Biochemistry and Biotechnology* 193, 1780 – 1799.
- [7] Chefer, H., Gur, S., Wolf, L., 2021. Transformer interpretability beyond attention visualization. *2021 IEEE/CVF Conference on Computer Vision and Pattern Recognition (CVPR)*, 782–791.
- [8] Chen, T., Kornblith, S., Norouzi, M., Hinton, G., 2020. A simple framework for contrastive learning of visual representations, in: *Proceedings of the 37th International Conference on Machine Learning*, pp. 1597–1607.
- [9] Cui, P., Wang, X., Pei, J., Zhu, W., 2019. A survey on network embedding. *IEEE Transactions on Knowledge and Data Engineering* 31, 833–852.
- [10] Dosovitskiy, A., Beyer, L., Kolesnikov, A., Weissenborn, D., Zhai, X., Unterthiner, T., Dehghani, M., Minderer, M., Heigold, G., Gelly, S., Uszkoreit, J., Houlsby, N., 2021. An image is worth 16x16 words: Transformers for image recognition at scale URL: <https://>

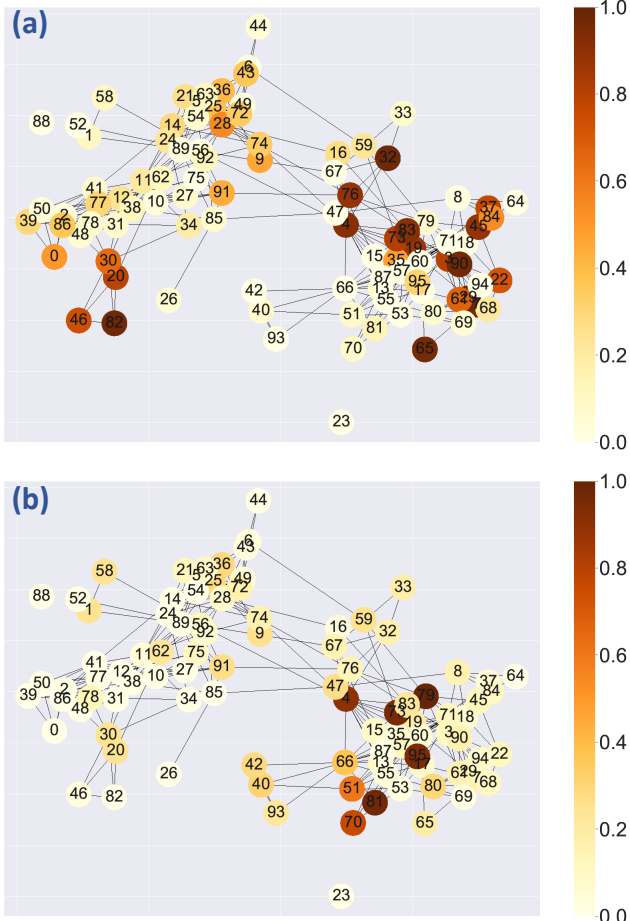


Figure 14: Co-occurrence interaction graphs of CholeraInf dataset with nodes coloured based on relevance scores of the LRP interpretation, which are summed across each state: (a) diarrhea period and (b) recovery period. The locations of states are obtained by clustering points of the graph embedding of the time-evolving graph via k -means. The dark brown colour indicates nodes with the highest importance for the decision-making of the model.

openreview.net/forum?id=YicbFdNTTy.

[11] Dwivedi, V.P., Bresson, X., 2021. A generalization of transformer networks to graphs. AAAI Workshop on Deep Learning on Graphs: Methods and Applications .

[12] Faust, K., Lahti, L., Gonze, D., de Vos, W.M., Raes, J., 2015. Metagenomics meets time series analysis: unravelling microbial community dynamics. Current opinion in microbiology 25, 56–66.

[13] Gehring, J., Auli, M., Grangier, D., Yarats, D., Dauphin, Y.N., 2017. Convolutional sequence to sequence learning, in: Precup, D., Teh, Y.W. (Eds.), Proceedings of the 34th International Conference on Machine Learning, PMLR. pp. 1243–1252. URL: <https://proceedings.mlr.press/v70/gehring17a.html>.

[14] Goyal, P., Kamra, N., He, X., Liu, Y., 2018. Dyngem: Deep embedding method for dynamic graphs. ArXiv abs/1805.11273.

[15] Goyal, P., Rokka Chhetri, S., Canedo, A., 2020. dyngraph2vec: Capturing network dynamics using dynamic graph representation learning. Knowl. Based Syst. 187. doi:10.1016/j.knosys.2019.06.024.

[16] Grover, A., Leskovec, J., 2016. Node2vec: Scalable feature learning for networks, in: Proceedings of the 22nd ACM SIGKDD International Conference on Knowledge Discovery and Data Mining, pp. 855–864. doi:10.1145/2939672.2939754.

[17] Hsiao, A., Ahmed, A.M.S., Subramanian, S., Griffin, N.W., Drewry, L.L., Petri, W.A., Haque, R., Ahmed, T., Gordon, J.I., 2014. Members of the human gut microbiota involved in recovery from vibrio cholerae infection. Nature 515, 423–426. doi:10.1038/nature13738.

[18] Jain, S., Wallace, B.C., 2019. Attention is not explanation, in: NAACL.

[19] Joossens, M., Huys, G., Cnockaert, M., Preter, V., Verbeke, K., Rutgeerts, P., Vandamme, P., Vermeire, S., 2011. Dysbiosis of the faecal microbiota in patients with crohn’s disease and their unaffected relatives. Gut 60. doi:10.1136/gut.2010.223263.

[20] Kazemi, S.M., Goel, R., Jain, K., Kobyzev, I., Sethi, A., Forsyth, P., Poupart, P., Borgwardt, K.M., 2020. Representation learning for dynamic graphs: A survey. J. Mach. Learn. Res. 21, 70:1–70:73.

[21] Langdon, A.E., Crook, N., Dantas, G., 2016. The effects of antibiotics on the microbiome throughout development and alternative approaches for therapeutic modulation. Genome Medicine 8.

[22] Melnyk, K., Klus, S., Montavon, G., Conrad, T.O., 2020. Graphke: graph kernel koopman embedding for human microbiome analysis. Applied Network Science 5. doi:10.1007/s41109-020-00339-2.

[23] Menni, C., Jackson, M.A., Pallister, T., Steves, C.J., Spector, T.D., Valdes, A.M., 2017. Gut microbiome diversity and high-fibre intake are related to lower long-term weight gain. International Journal of Obesity 41, 1099–1105. doi:10.1038/ijo.2017.66.

[24] Mottawea, W., Chiang, C.K., Mühlbauer, M., Starr, A., Butcher, J., Abujamel, T., Deeke, S., Brandel, A., Zhou, H., Shokralla, S., Hajibabaei, M., Singleton, R., Benchimol, E., Jobin, C., Mack, D., Figeys, D., Stintz, A., 2016. Altered intestinal microbiota–host mitochondria crosstalk in new onset crohn’s disease. Nature Communications 7.

[25] Mukherjee, A., Chettri, B., Langpoklakpam, J.S., Basak, P., Prasad, A., Mukherjee, A.K., Bhattacharyya, M., Singh, A.K., Chattopadhyay, D., 2017. Bioinformatic approaches including predictive metagenomic profiling reveal characteristics of bacterial response to petroleum hydrocarbon contamination in diverse environments. Scientific Reports 7. doi:10.1038/s41598-017-01126-3.

[26] Narayanan, A., Chandramohan, M., Venkatesan, R., Chen, L., Liu, Y., Jaiswal, S., 2017. graph2vec: Learning Distributed Representations of Graphs. ArXiv doi:10.1145/1235.

[27] Parida, S., Sharma, D., 2021. The microbiome and cancer: Creating friendly neighborhoods and removing the foes within. Cancer Research 81, 790–800. doi:10.1158/0008-5472.CAN-20-2629.

[28] Perozzi, B., Al-Rfou, R., Skiena, S., 2014. Deepwalk: Online learning of social representations, in: KDD ’14: Proceedings of the 20th ACM SIGKDD international conference on Knowledge discovery and data mining, pp. 701–710. doi:10.1145/262330.2623732.

[29] Sankar, A., Wu, Y., Gou, L., Zhang, W., Yang, H., 2020. Dysat: Deep neural representation learning on dynamic graphs via self-attention networks, in: Proceedings of the 13th International Conference on Web Search and Data Mining, pp. 519–527.

[30] Shaw, L.P., Bassam, H., Barnes, C.P., Walker, A.S., Klein, N., Balloux, F., 2019. Modelling microbiome recovery after antibiotics using a stability landscape framework. The ISME Journal 13, 1845 – 1856.

[31] Shervashidze, N., Schweitzer, P., van Leeuwen, E.J., Mehlhorn, K., Borgwardt, K.M., 2011. Weisfeiler-Lehman Graph Kernels. Journal of Machine Learning Research 12, 2539–2561.

[32] Sun, K., Marasović, A., 2021. Effective attention sheds light on interpretability, in: Findings of the Association for Computational Linguistics: ACL-IJCNLP 2021, Association for Computational Linguistics, Online. pp. 4126–4135. URL: <https://aclanthology.org/2021.findings-acl.361>. doi:10.18653/v1/2021.findings-acl.361.

[33] Sánchez-Alcohalado, L., Ramos-Molina, B., Otero, A., Laborda-Illanes, A., Ordóñez, R., Medina, J., Gómez-Millán, J., Queipo-Ortuño, M., 2020. The role of the gut microbiome in colorectal cancer development and therapy response. Cancers 12. doi:10.3390/cancers12061406.

[34] Vashishth, S., Upadhyay, S., Tomar, G.S., Faruqui, M., 2019. Attention interpretability across nlp tasks. ArXiv abs/1909.11218.

- [35] Vaswani, A., Shazeer, N., Parmar, N., Uszkoreit, J., Jones, L., Gomez, A.N., Kaiser, L., Polosukhin, I., 2017. Attention is all you need, in: Proceedings of the 31st International Conference on Neural Information Processing Systems, p. 6000–6010. doi:10.5555/3295222.3295349.
- [36] Veličković, P., Cucurull, G., Casanova, A., Romero, A., Liò, P., Bengio, Y., 2018. Graph Attention Networks. International Conference on Learning Representations URL: <https://openreview.net/forum?id=rJXMpikCZ>.
- [37] Voita, E., Talbot, D., Moiseev, F., Sennrich, R., Titov, I., 2019. Analyzing multi-head self-attention: Specialized heads do the heavy lifting, the rest can be pruned, in: Proceedings of the 57th Annual Meeting of the Association for Computational Linguistics, Association for Computational Linguistics, Florence, Italy. pp. 5797–5808. URL: <https://www.aclweb.org/anthology/P19-1580>.
- [38] Zhang, D., Yin, J., Zhu, X., Zhang, C., 2020. Network representation learning: A survey. IEEE Transactions on Big Data 6, 3–28.